HHS Public Access

Author manuscript

J Mol Biol. Author manuscript; available in PMC 2015 April 03.

Published in final edited form as:

J Mol Biol. 2014 April 3; 426(7): 1554–1567. doi:10.1016/j.jmb.2013.12.027.

Evidence against the 'Y-T coupling' mechanism of activation in the response regulator NtrC

Janice Villali[1], **Francesco Pontiggia**[1], **Michael W. Clarkson**[1], **Michael F. Hagan**[2], and **Dorothee Kern**[1,*]

[1]Department of Biochemistry and Howard Hughes Medical Institute, Waltham, Massachusetts 02452, USA

[2]Department of Physics, Brandeis University, Waltham, Massachusetts 02452, USA

Abstract

The dominant theory on the mechanism of response regulators activation in two-component bacterial signaling systems is the 'Y-T coupling' mechanism, wherein the χ_1 rotameric state of a highly conserved aromatic residue correlates with the activation of the protein via structural rearrangements coupled to a conserved tyrosine. In this paper we present evidence that in the receiver domain of the response regulator Nitrogen Regulatory Protein C ($NtrC^R$) the interconversion of this tyrosine (Y101) between its rotameric states is actually faster than the rate of inactive/active conversion and is not correlated to the activation process. Data gathered from NMR relaxation dispersion experiments show that a subset of residues surrounding the conserved tyrosine sense a process that is occurring at a faster rate than the inactive/active conformational transition. We show that this process is related to χ_1 rotamer exchange of Y101 and that mutation of this aromatic residue to a leucine eliminated this second faster process without affecting activation. Computational simulations of $NtrC^R$ in its active conformation further demonstrate that the rotameric state of Y101 is uncorrelated with the global conformational transition during activation. Moreover, the tyrosine does not appear to be involved in the stabilization of the active form upon phosphorylation, and is not essential in propagating the signal downstream for ATPase activity of the central domain. Our data provides experimental evidence against the generally accepted 'Y-T coupling' mechanism of activation in $NtrC^R$.

Introduction

Two-component systems are the predominant signaling systems in bacteria, allowing them to react to a wide variety of changes in their cellular environment. A basic two-component system consists of a histidine kinase whose conserved C-terminal transmitter domain

*To whom correspondence should be addressed: dkern@brandeis.edu.
Current address for M.C: Bio Med Molecular Pharmocology, Physiology, and Biotechnology, Brown University, Providence, RI 02912

becomes phosphorylated in response to a signal in the variable sensor domain. The histidine kinase's cognate response regulator can then catalyze the phosphoryl-transfer to its own conserved aspartate residue. In the response regulator Nitrogen Regulatory Protein C (NtrC), which activates transcription of a number of genes under conditions of limited nitrogen supply, the receiver domain is in a pre-existing equilibrium between the active and inactive substates in the wildtype protein.[1] When its associated histidine kinase, NtrB, is phosphorylated due to low intracellular nitrogen concentrations, the subsequent transfer of the phosphate to the receiver domain of NtrC causes a shift in this pre-existing equilibrium far toward the active state through active state stabilization.[2] The structural change in the region of α-helix 3 through β-strand 5 ('3445 face') in the receiver domain ($NtrC^R$) modifies its interaction with the central domain of NtrC[3], leading to oligomerization of the full length protein[4], ATPase activity[5], and the activation of the σ^{54} promoter through a DNA looping mechanism.[6]

The activation mechanism of response regulators has gained much attention due to its central role in bacterial signaling and its early recognition as a classical system to study allostery in single domain proteins.[7] Because our new results presented here rule out the popular 'Y-T coupling' mechanism[8], we briefly review previous publications on this topic. Crystal structures of the homologous response regulator CheY led researchers to propose the 'Y-T coupling' mechanism of activation, which is reminiscent of an induced fit view of allostery.[8] The Y and T in question are Y101 and T82 ($NtrC^R$ numbering) which are highly conserved as either a tyrosine or phenylalanine, and as a threonine or serine, respectively, in response regulators.[9] A crystal structure of the BeF_3^- phosphate analog activated receiver domain of CheY showed that the position of the threonine was coupled to the χ_1 rotameric state of the tyrosine when compared to the unphosphorylated inactive protein.[8] In both a low resolution[10] and a high resolution[11] structure of CheY, in the inactive state the tyrosine was found to be occupying both the *g+* and *t* rotameric states while in activated CheY the threonine moved to coordinate the phosphate group, leaving a gap in the side chain packing. Tyrosine was then thought to fill this gap by going exclusively into the *t* state and becoming buried in the interior of the protein. This mechanism was also supported by the crystal structures of a series of mutations of the threonine and tyrosine, in which the rotameric state of the aromatic ring corresponded to whether or not the mutants were able to function properly during chemotaxis assays in *E coli*.[12] In 2006, Dyer and Dahlquist solved a crystal structure of unphosphorylated CheY with a fragment of its target protein, FliM.[13] They found that although the tyrosine was buried in the interior of the protein, the threonine, as well as the loop between β-strand 4 and α-helix 4 (β4/a4 loop), appeared to be only midway to the activated state. Analysis of all known structures of CheY led to the proposal that before phosphorylation the tyrosine was free to move independently from the threonine and the b4/a4 loop region, but upon phosphorylation, the threonine acted as a gate to the loop motion leading to a correlated movement of the tyrosine rotating to the buried *t* state. The authors dubbed this mode of allosteric activation 'T-loop-Y coupling'.[13; 14] Importantly, activation coupled to the rotameric state of the tyrosine has been proposed to be a general mechanism of response regulator activation based on the tyrosine having distinct states in the inactive and active structures of a number of different response regulators.[15; 16; 17; 18; 19]

Besides these experimental studies, many computational studies have been carried out on various receiver domains of response regulators with controversial results. Although this tyrosine was seen to be undergoing free rotameric rotation in the inactive state in molecular dynamics (MD) simulations in CheY, the motion of the β4/a4 loop and the tyrosine were reported to be correlated in simulations of the active conformation.[20] A similar result was found for FixJ where the β4/α4 loop and phenylalanine appeared to be correlated but the threonine movement was not[21]. In a more recent paper, the tyrosine was shown to be coupled to both the threonine and the β4/a4 loop using a statistical mechanics model of protein allostery in CheY.[22] In $NtrC^R$, elastic network modeling found that motions encompassing the aspartate that becomes phosphorylated, as well as the threonine and the tyrosine, were all correlated.[23] Pandini et al also found support for a pre-organized network of allosteric connections between these residues and the functional site of phosphorylation.[24] Alternatively, transition path sampling in combination with potential mean force calculations found that the energy barrier of tyrosine/phenylalanine rotamer exchange was lower than the barrier involved in the inactive/active transition, making the rotameric state of the conserved aromatic residue kinetically independent from the functional conformational transition, and leading them to theorize a role for the tyrosine in the thermodynamic stabilization of the active substate[25; 26].

Early NMR experiments to probe protein dynamics gave a hint that the tyrosine may not be directly coupled to the motion of the inactive/active transition. Dynamics on the microsecond to millisecond timescale were seen in residues surrounding Y101 in the phosphorylated form of $NtrC^R$ however, the applied model-free analysis did not allow us to quantitatively characterize conformational exchange processes.[1] Microsecond to millisecond motion has also been seen in phosphorylated CheY, with the majority of it localized to the area encompassing the β4/α4 loop and the tyrosine.[27] Despite the plethora of contradicting computational and experimental studies involving the role of the highly conserved tyrosine in the mechanism of activation of response regulators, 'Y-T coupling' is the dominant description of activation for these systems.[14; 17; 18; 28]

Here we use NMR relaxation dispersion experiments in combination with molecular dynamics simulations to provide evidence that Y101 in $NtrC^R$ moves independently, and more quickly than the inactive/active conformational transition both before, and after, the addition of the BeF_3^- phosphate analog. By experimentally characterizing a Y101L mutant, we demonstrate directly, that Y101 is not needed for the inactive/active transition and that it does not thermodynamically stabilize the active state structure. This data challenges the prevailing description of the activation of allosteric response regulators.

Results and Discussion

Y101 rotameric state is kinetically independent from the inactive to active transition

Using ^{15}N NMR CPMG (Carr-Purcell-Meiboom-Gill) relaxation dispersion experiments originally described by Loria et al.[29] and Vallurupalli et al.[30], in combination with an independently determined exchange-free transverse relaxation rate[31], we determined the existence of a second dynamic process in $NtrC^R$, in addition to the previously described inactive/active transition.[2] For a resonance undergoing exchange, the transverse relaxation

rate (R_2^{eff}) is equal to the intrinsic rate of relaxation (R_{20}) plus an additional rate of relaxation due to exchange (R_{ex}). The latter can be suppressed by an external magnetic field, a phenomenon that has extensively been used to quantify conformational exchange processes in the millisecond to high microsecond time regime in CPMG experiments[29; 32;33]. Typical CPMG relaxation dispersion profiles are shown in Fig. 1 A-C, where increasing CPMG frequencies (ν_{CPMG}) are applied to suppress the R_{ex} component of R_2^{eff} with full suppression at the highest field strength of 1000 Hz that should correspond to the exchange-free transverse relaxation rate.[29] These data are routinely fit to an equation describing a two-site exchange process to obtain the corresponding rates. However, we discovered that for a number of residues, the seeming exchange-free relaxation rate determined from the CPMG experiments ($R_2\beta_{1000Hz}$) is actually not the true $R_{20}\beta$ by measuring the latter via a combination of three TROSY based NMR relaxation experiments as described in detail elsewhere.[31] These values are significantly lower (shown as values for $\nu_{CPMG\rightarrow\infty}$) than the one predicted from the CPMG curves, revealing a second dynamic process.

We note that this “hidden” second process could not be unambiguously identified for unphosphorylated wildtype $NtrC^R$ (WT) because its rate of inactive/active interconversion is ~14,000 s^{-1}; too fast to be suppressed by the maximum CPMG field strength of 1000 Hz.[2] However, for unphosphorylated S85D, Y101F along with WT activated by the phosphate mimic BeF_3^-, the inactive/active transition is slow enough[2] to separate the dynamics of the activation step from the faster second process.

By comparing $R_2\beta_{1000Hz}$ and $R_{20}\beta$ we were able to probe on a per-residue basis both dynamic processes. The values for $R_2\beta_{1000Hz}$ and $R_{20}\beta$ calculated for most amides agree well with each other, but a small percentage of residues in S85D, Y101F, and BeF_3^- -activated $NtrC^R$ have $R_2\beta_{1000Hz}$ values significantly higher than the corresponding $R_{20}\beta$ (Fig. 1D-F). This provides evidence that in $NtrC^R$ a second faster exchange process is sensed in a subset of residues, which is not fully suppressed in the CPMG experiment, and which does not have any perceptible effect on the CPMG dispersion curves itself. Interestingly, the amino acids with exchange from both processes (orange, Fig. 2G) cluster around Y101 (blue) suggesting that this second faster process is linked to Y101 dynamics. Furthermore, it implies that this movement is unrelated to the inactive/active interconversion, in sharp contrast to the dominant ‘Y-T coupling mechanism’.

Y101L mutant verifies that the faster dynamic process is due to rotamer exchange

In order to test this hypothesis, we mutated Y101 to a leucine. This might be considered a dramatic substitution, as the residue in position 101 is typically conserved as either a tyrosine or a phenylalanine in the NtrC family, with only less than 2% of occurrences as leucines and high conservation across response regulators (Figure S4A). The Y101L $NtrC^R$ mutant could be expressed and purified with no apparent differences in expression levels or stability compared to WT. A backbone amide ^{15}N-CPMG dispersion experiment was carried out on the Y101L mutant and the residues undergoing exchange were fit globally with a rate of exchange equal to 2,200 ± 300 s^{-1} (Figure 2A), similar to the rate constants of Y101F.[2]

Strikingly, the second fast process is absent in Y101L as determined by the fact that the $R_{20}\beta$'s and $R_2\beta_{1000Hz}$ values from the CPMG experiments are identical (Fig. 2 A, B). Only one residue has a statistically significant difference in value of $R_{20}\beta$, residue S13. This serine is located in a loop near the phosphorylation site, next to D10 and D11 that help in the coordination of a Mg^{2+} ion upon phosphate binding. Since S13 is far from position 101, it is reasonable to hypothesize that S13 is not sensing the second fast process in WT, but possibly the binding and release of positively charged sodium ions in the buffer.

Two additional observations from the NMR spectra of the Y101L mutant are worth mentioning. First, the equilibrium of the two conformational substates is shifted more toward the inactive state (Fig. 2C), as revealed by the peak position relative to WT and an activating mutant D86N/A89T.[1] Second, residues with dispersion were not only found on the '3445 face', as in previously studied WT, mutants, and activated-$NtrC^R$, but were also observed along α-helix 5. By removing the aromatic sidechain from the residue at position 101 in $NtrC^R$, α-helix 5 now appears to be able to sense the dynamics of the activation transition. We note that chemical shift differences between states do not mean that these residues move, but rather that this nucleus has different electronic environments in the exchanging states. A change in the allosteric network upon mutation of the conserved aromatic group has been observed previously in the receiver domain of RegA, with new dynamics measured in α-helix 1 with a constitutively active tryptophan mutation.[34]

In summary, NMR experiments on Y101L and BeF_3^--activated WT $NtrC^R$ provide confirmation that the interconversion between rotameric states of Y101 is the cause of the discrepancy in $R_{20}\beta$ and $R_2\beta_{1000Hz}$ values in S85D, Y101F, and BeF_3^- -activated $NtrC^R$. The rate of the tyrosine flip is faster than the measured rate of the inactive/active conformational change, even in the activated protein, signifying that 'Y-T coupling' is not rate-limiting in the activation mechanism of $NtrC^R$.

MD simulations identify rotameric exchange as independent from activation dynamics

To gain more insight at an atomistic level on the nature of the fast motion involving Y101, its correlation with T82, and the connection of this motion with the global active to inactive state interconversion, we performed a long unbiased MD simulation of the apo active conformation of $NtrC^R$ using the supercomputer Anton. During the 71 μs long simulation we observe that the side chain of tyrosine 101 is not locked in a single conformation, but alternatively interconverts among the three accessible rotameric states (Fig. 3A). The three rotameric states have relative populations of approximately 0.68, 0.28, and 0.04, for the *t*, *g*+ and *g*− states, respectively, and the typical residence time in the most populated one is on the order of 1 μs (see Fig. S1A). The state with the largest population, state *t*, not surprisingly corresponds to the χ_1 angle that is most often associated with the active state X-ray structures of response regulators (Fig. 3D, green).

MD simulations can directly address the question of correlated motions that cannot be directly extracted from ensemble-averaged experiments. The simulation shows no strong correlation between the motions of Y101 and T82. The side-chain of T82 remains in the same rotameric state for almost the entire length of the simulation, independent of the position of Y101 (Fig 3B). Interestingly, it is only when Y101 is completely moved away

from the active site, as in the minor state *g*−, that T82 has the freedom to explore all three side-chain rotamers with sizable probability (Fig. S1B). The key result from the simulations is that despite the different conformations attained by Y101 and T82, the rotation of α–helix 4 around its axis, which reports on the crucial change in the solvent exposure of L87, A90, and V91 and is important in downstream signaling, remains in the active conformation throughout the simulation (Fig 3C). This long unbiased MD simulation delivered crucial information about the atomistic details of the Y101 dynamics as well as information about the question of correlated motions, neither of which could be addressed directly by experiments.

Using a combination of computation and experimental data we have shown that the fast timescale motion of Y101 is a rotamer interconversion that is uncorrelated with the global conformational transition that the '3445' signaling face experiences during the activation/inactivation process in $NtrC^R$, and not correlated to the T82 dynamics, ruling out a Y-T activation mechanism for NtrC as had been proposed in earlier studies.[19] In this context it is important to point out that the structural description of active and inactive conformers in $NtrC^R$ is quite different from the one typically used when discussing receiver domains of other response regulators. In CheY the structural variation between the active and inactive conformers is more localized than in NtrC and can be described by changes in the positions of a handful of residues, including T82, Y101 and the loop between β-strand 4 and α-helix 4, whereas the conformation attained by α–helix 4 is nearly identical in the two conformers.[35] In $NtrC^R$, a more global conformational change occurs and this global change is essential for signal propagation. For this reason, the rotameric state of Y101 may be less important in the activation mechanism and downstream signaling of $NtrC^R$ as compared to other response regulators, such as CheY.

Comparison between NMR experiments and MD simulations

The MD simulations on activated apo $NtrC^R$ suggest that the second faster process detected by the NMR relaxation experiments may be a rotamer exchange of Y101, in agreement with the NMR data on Y101L. Three bond J-coupling values deliver valuable information about the χ1 rotamer angles of aromatic residues by NMR.[36] To test our hypothesis, we determined the $^3J_{NC\gamma}$ value for Y101 in BeF_3^--activated WT $NtrC^R$ to be 1.6 +/ 0.2 Hz, where gauche χ1 angles cluster around 0.5 Hz and trans angles cluster around 2.4 Hz. Aromatic residues that sample more than one rotamer in the fast NMR time regime will have an intermediate value. The $^3J_{NC\gamma}$ for Y101 in the activated state is consistent with the tyrosine sampling multiple rotamers with a higher population of the trans state as seen in the MD simulations (Fig. 3A).

From the NMR relaxation data a rough estimate of the rate constant of about 30,000 ± 12,000 process was determined for BeF_3^--activated $NtrC^R$ (see supplemental material). We want to note that it is impossible to separate populations from delta omegas in the fast exchange limit. In principle, one could try to estimate the chemical shift difference from the MD simulations and use this information as input for fitting the NMR data. While qualitatively chemical shift perturbations estimated from the MD simulations using Sparta +[37] are in the same regions as detected by NMR (Fig. S2), this approach does not yield

reliable quantitative results (Fig. S3), reaching the existing current limits in our methods. In the MD simulations three different rotameric states are being sampled with different lifetimes. First, even with a 71 μs simulation, insufficient sampling hampers accurate estimations of populations and rate constants. Second, a multi-state conformational exchange on this timescale cannot be quantitatively dissected from the NMR experiments. Third, the slower and the faster processes measured by NMR superimpose for many residues, and both processes are not necessarily uncorrelated. For these reasons we prefer not to over interpret our data and only calculated a rough estimate of the second process.

Aromatic rotamer dynamics in proteins has been extensively studied and continues to be a topic of interest. MD and fluorescence studies on rotamer exchange on small peptides have found rates of interconversion for aromatic residues on the nanosecond timescale[38], but the variability in packing of aromatic residues in proteins can lead to a large range of ring flipping frequencies, spanning from the minutes to the subnanosecond timescale, even within the same protein.[39; 40; 41;42] In our MD simulation, F99 does not rotate, whereas Y122 rotates in sub-microseconds within $NtrC^R$.

Mutating the conserved aromatic does not affect activation and NtrC's downstream ATPase activity

As previously mentioned, the amino acid corresponding to position 101 in $NtrC^R$ is predominantly an aromatic amino acid in all receiver domains throughout the whole two-component system superfamily. Specifically, for NtrC, that amino acid is a tyrosine or phenylalanine in approximately 90% of the sequences classified as NtrC in the prokaryotic two-component systems database,[43] with only few occurrence of other amino acids (Fig S4A). Other subfamilies, such as CheY, CheV and CheB, show a slightly higher variation (Fig S4B-D), but in all analyzed response regulators families, the residue has an aromatic side chain in about 85% of the sequences (Fig S4F). The high level of conservation, together with the available structural information of active and inactive conformers, led researchers to identify the tyrosine as crucial trigger in the activation mechanism of the receiver domain of response regulators.[8] However we have shown here that the conformational changes that Y101 undergoes are not related to the global conformational rearrangement hallmark of the activation of NtrC.

It is instead possible that, as suggested by other studies,[25; 26] the aromatic residue in position 101 is needed thermodynamically in the stabilization of the active state once the protein becomes phosphorylated. To test this we activated Y101L $NtrC^R$ with BeF_3^-, a ground state phosphate mimic that has been shown to activate $NtrC^R$ to the same extent as phosphate.[19; 44] An [$^1H^{15}N$]-HSQC overlay of BeF_3^- -Y101L with BeF_3^- -WT protein show similar spectra, with the peak positions confirming that the activated Y101L mutant shifts its population toward the active state similarly to WT (Fig. 4B). BeF_3^- -activated Y101L $NtrC^R$ also shows an exchange rate comparable to BeF_3^--activated $NtrC^R$ (1,500 ± 600 s^{-1} and 1,950 ± 290 s^{-1} respectively) (Fig. 4A). These results imply that stabilization of the active state is also not dependent on the conserved tyrosine residue.

Since we have shown that Y101 is not necessary for the kinetics or thermodynamics of the functional conformational change in the receiver domain of $NtrC^R$, the next logical

possibility to investigate is a potential crucial role of this conserved aromatic residue in the propagation of this structural change to the next step in the signaling cascade. Stabilization of the active conformation upon phosphorylation exposes a group of hydrophobic residues (L87, A90, and V91) on the '3445 face' which have been suggested to be the contact sites between the receiver domain and the central domain of NtrC.[19] This central domain is responsible for both the oligomerization and ATPase activity of the protein, leading to the activation of the σ^{54}-holo enzyme transcription factor. To assess the role of Y101 in the signal transduction between receiver and central domain, we measured and compared the ATPase activity of BeF_3^- -activated full-length WT and Y101L NtrC using a colorimetric assay that measures the amount of inorganic phosphate released due to ATP hydrolysis (Fig. 4C). The results show that BeF_3^- -activated Y101L NtrC has only a small decrease in the rate of ATP hydrolysis compared to WT indicating that an aromatic residue at position 101 is not essential for transducing the signal to the downstream central domain of the protein.

Similar mutational studies on the activity of homologous response regulators have been carried out previously on CheY and OmpR. A study by Zhu et al.[45] on CheY looked at the effect of mutations on the ability of CheY in *E. coli* to direct flagella rotation by monitoring swimming and tumbling during chemotaxis. They found that replacement of the tyrosine by a tryptophan led to a hyperactive phenotype. The mutation to a phenylalanine, conversely, created a phenotype that had very low activity, while the leucine, valine, isoleucine, and glycine mutations resulted in no measureable activity at all. In an X-ray crystal structure of a constitutively active mutant, D13K/Y106W, bound to a peptide of its downstream interaction partner, FliM, CheY was found to be bound to FliM and in the active conformation in two of the four molecules in the asymmetric unit, while the other two molecules were unbound and in the inactive conformation.[46] In the Y106W single mutant structure, however, CheY was found to be in the active form in the absence of peptide.[12] Based on these results, the authors suggested that there might be a low energetic barrier between the inactive and active conformations in CheY, which includes the conserved aromatic residue. This barrier may increase once the protein is bound to its downstream target, FliM.[38] In the OmpR system, which is involved in osmotic regulation, a mutation of the conserved tyrosine to a cysteine resulted in a constitutively active protein as monitored by gene expression.[47] This mutation also caused an increase in the ability of OmpR to bind to its cognate DNA *in vitro*. Interestingly, in both of these cases, the rate of phosphorylation and dephosphorylation of the mutant proteins remained the same as for WT suggesting that the difference in activity may not be caused by the receiver domain activation but by the domain's ability to transmit the signal downstream.

Conclusion

The activation mechanism of $NtrC^R$ appears to be quite different from what has been previously proposed.[8; 13] Our data, together with others'[1; 25; 26; 27], shows in fact that the 'Y-T coupling' model of activation, inferred mainly from structural differences in the highly conserved Y101 between the active and inactive conformations of various response regulators, is not valid for NtrC. The motion of Y101 is uncorrelated to the global conformational rearrangement and the aromatic side-chain is not needed for the stabilization of the activated state by BeF_3^- or for activating the central domain ATPase. These

observations highlight the fact that by looking beyond static structures and focusing further on ensembles that correspond to the inherent dynamics in proteins, more accurate predictions about whether, and how, specific residues are implicated in function may be obtained. Although harder to come by, information about structures and kinetics of lowly populated states along the transition have the possibility of providing a wealth of information that is not accessible by looking only at the more highly populated ground states that are typically captured in structural biology.

NMR dynamics experiments are becoming widely used to ascertain information about the interplay between protein motion and function.[48; 49; 50] Our results illustrate that interpreting dynamic data can be complicated when more then one dynamic process is present, which is a common trait of biological systems. In some cases three-state models can be quantified by combining multiple CPMG dispersion experiments[51] or by doing the experiments at multiple field strengths and temperatures[52; 53; 54; 55; 56], but in those cases the R_2^{eff} is fully suppressed by the maximum field strength. By measuring the exchange free transverse relaxation, in addition to CPMG dispersion for $NtrC^R$, we were able to separate the inactive to active conformational transition from an independent tyrosine rotation for residues where R_2^{eff} was not fully suppressed. In addition, we used the single molecule characteristic of molecular dynamics simulations to address the question of correlated motions. Recently, CPMG NMR dispersion experiments on non-phosphorylated CheY were fit to a strict two-state model, where Y101 was fit to a slightly faster rate compared to other residues.[57] The data were interpreted with a model of inactive to active switching in a non-concerted sequential fashion with a possible preferred sequential order. In light of our results presented here, we wonder if the CPMG data on CheY reflect a similar dynamic mechanism where the tyrosine rotation is a second independent process from the activation, as we have described on NtrC. Separating these different motions, by acquiring additional dynamics data, might give more insight into the possible multiple motions that CheY is experiencing and better assign a biological role to these processes.

This new information on the activation mechanism of response regulators stimulates further questions regarding the reason why this aromatic residue is so highly conserved in this family of proteins. As already shown in CheY,[45] and also seen in our work on NtrC, replacing the tyrosine with a non-aromatic residue does not impair the ability of the receiver domain to be phosphorylated. Moreover, we have shown that the receiver domain of NtrC lacking Y101 is able to transfer the signal to the next downstream partner, the central ATPase domain. Based on these observations, we speculate that the tyrosine may play a role in interactions with further downstream partners, such as the σ^{54}-holoenezyme transcription factor. This hypothesis is in line with activity data in both CheY and OmpR, where mutating the tyrosine led to a change in functionality at the cellular level. It is also possible that the aromatic residue is important to interactions with other regulatory domains in some two-component systems, such as the P2 domain on CheY's associated histidine kinase, CheA[58] or with associated phosphatases.[59] Our results underscore the importance of determining the biological roles of specific dynamic processes. This new perspective on the activation mechanism and signal propagation in $NtrC^R$ could provide new insights into two-component signaling in bacteria and regulation by allosteric proteins in general.

Methods

NMR sample preparation

Unlabeled and uniformly ^{15}N-labeled NtrC^{R} wild-type, mutant, and BeF_3^- activated forms were prepared as previously described. [1; 19] S85D and Y101F NtrC^{R} NMR samples were 0.75 mM in 50 mM Na_3PO_4 buffer, pH 6.75 with 10% D_2O. Y101L, BeF_3^- Y101L, and BeF_3^- WT NtrC^{R} samples were 0.3 mM to avoid transient aggregation.

NMR experiments

TROSY ^{15}N relaxation dispersion experiments were acquired on Varian Inova 600 MHz spectrometer at 298K. Constant time T_2 delays between 60 and 70 ms were used in all TROSY CPMG dispersion experiments,[29; 60; 61; 62] which roughly yielded 55% of residual signal intensity, and CPMG field strengths between 28 and 1000 Hz were collected. Data was processed using NMRPipe[63] and the change in R_2^{eff} with increasing frequency of CPMG refocusing pulses were fit globally for each mutant to the fast form of the Carver-Richards equation (R_2^{eff} (ν_{CPMG}) = $R_{20}\beta(\nu_{CPMG\rightarrow\infty})$ + ($p_I p_A \Delta\omega^2_{IA}/k_{ex}$)[1-($4\nu_{CPMG}/k_{ex}$)tanh($k_{ex}/4\nu_{CPMG}$)]) in Matlab. The variation of R_{ex} with an increasing applied radio-frequency field (ν_{CPMG}) permits the CPMG dispersion experiment to quantitatively determine kinetics (k_{ex}) for a two-state exchange process[29; 61] even for highly skewed populations.[60] Noise estimated from flat residues was used as an input for Monte-Carlo simulations in MatLab to determine the error in the fitted parameters.

In a TROSY-based experiment the exchange free component relaxes with the rate $R_{20}\beta$ where $R_{20}\beta=R_{20}-\eta_x+R_1^H/2$. η_{xy} is the cross correlation between the ^{15}N-^{1}H dipolar interactions and the ^{15}N chemical shift anisotropy, which can be measured by determining the ratio of peak intensity for the I_β/I_α using a pulse sequence developed by Wang *et al.*[64] R_1^H can be estimated through $R_1^H \sim R_1^{HzNz} - R_1^N$ using both a TROSY pulse sequence to calculate R_1^{HzNz} and a standard experiment to measure the longitudinal relaxation on each amide nitrogen (R_1^N).[65] The combination of these three experiments allows one to calculate the independently determined $R_{20}\beta$.[31]

The exchange-free transverse relaxation time of the TROSY component was determined using pulse sequences designed to measure R_2^α and R_2^β with a 2τ delay of 43.2 ms to ensure a ratio $I^\beta/I^\alpha \sim 0.3$ for most residues, and R_1^{2HzNz} with a τ delay of 21.6 ms.[31;64] ^{15}N R_1 values were measured using standard experiments[65] with the following T_1 delays: 0.01, 0.1, 0.5, 0.7, 1.1, 1.5 s. R_1^H values were measured using a TROSY-based R_1^{HzNz} pulse sequence (L.E. Kay, personal communication) employing a reburp pulse to selectively invert the amide region with following delay times: 0.025, 0.04, 0.06, 0.1, 0.15, 0.2, 0.3, 0.35 s. Data was processed using NMRPipe. Intensities were fit to a mono-exponential decay curve, and uncertainties were measured from duplicate points and an estimate of signal-to-noise (2%).

$^3J_{NC\gamma}$ couplings for aromatic and residues were obtained from quantitative *J*-correlation spectroscopy[36] in duplicate with a dephasing time of 50 ms.

ATPase activity assays

Full-length dimeric WT and Y101L NtrC with 3 alanine mutations in the c-terminal domain to prevent higher order oligomerization upon activation[66] were grown as described previously.[66] Cells were resuspended in buffer (50mM TrisOAc, pH 8.2, 50mM KCl, 10% v/v glycerol, 0.02% NaN_3, and 0.4mM TCEP) and lysed using 1mg/mL lysozyme (Sigma) at 25°C for one hour. Cleared lysates were precipitated by a 0-35% $(NH_4)_2SO_4$ saturation and were further purified by ion exchange chromatography using a Q Sepharose Fast Flow column (50 mM TrisHCl, pH 7.5, 20 mM NaCl, 0.4 mM TCEP) with a 1M NaCl gradient over 8 column volumes for elution. Rates of ATP hydrolysis were determined using a colorimetric malachite green assay[67] in order to detect released inorganic phosphate (linear range 0.2-40 μM). Reactions were carried out in triplicate in a 96 well plate using malachite green reagents (Bioassay Systems) and KH_2PO_4 as the standard. Briefly, 1 μM final dimeric NtrC was mixed in with assay buffer (50 mM HEPES·KOH, pH 7.3, 100 mM KOAc, 8 mM $Mg(OAc)_2$, and 5 mM β-ME) in the presence and absence of 200μM $BeCl_2$ and 5 mM NaF and incubated at room temperature for 5 minutes. Following the addition of 0.1mM equimolar Mg^{2+}ATP, pH 7.0, 80 μL aliquots were taken at 30 second intervals and quenched in 20 μL of the reaction solution (0.337 g Malachite green in 750 mL of HPLC grade H2O combined with 10.5 g ammonium molybdate (Sigma) in 250 mL of 4N HCl). The formation of the reactant malachite green/molybdate/Pi complex was measured by absorbance at 620 nm after incubation at room temperature for 30 minutes to allow for color development.

Molecular simulations

The active structure of the receiver domain of NtrC, refined in a previous study in our lab,[68] was used as starting structure for the simulation. The system was parameterized with the CHARMM 22-protein all-atom force field with the CMAP backbone energy correction included[69; 70] using the psfgen plugin in VMD.[71] The system was solvated in a rectangular box with TIP3 water molecules and neutralized with 7 sodium ions. The simulation box therefore contained approximately 24,600 atoms. Periodic boundary conditions were applied to the simulation box. After energy minimization, the simulation box was gradually heated to 310 K with a time step of 1 fs while gradually releasing positional restraints in a MD simulation of 2 ns with the software NAMD 2.7b2.[72] The system was equilibrated for an additional 70 ns in the NPT ensemble (T = 310 K, P = 1.01325 bar) with the software NAMD, using the Langevin dynamics method[73] for temperature control, and the combined Langevin piston Nose-Hoover method[74; 75] for controlling pressure.

Further testing and the production run were then performed on the supercomputer Anton, designed and produced by DESRES research.[76] The final configuration of the NAMD trajectory was converted to run on Anton using a set of scripts provided by the staff at PSC and tests were performed to evaluate performance and accuracy and to tune the parameters for the run. The final parameters used for the production runs on Anton were a timestep of 2.5 fs, a 32×32×32 FFT mesh and a 1:1:2 RESPA scheme. With those parameters, the energy drift rate in test NVE simulations was approximately 0.017 Kcal/mol/Dof/us, which for our system (~ 50000 dof) matches DESRES published results for similar systems.[77] In all subsequent runs the systems were coupled to a Nose-Hoover thermostat.

The performance of the runs was about 12 μs/day. After a first exploratory run at 310K (data not shown) for ~12 μs the system was reintroduced to NAMD, re-equilibrated to 320K, reconverted to Anton and simulated at 320K for approximately 71.5 μs.

The pseudoangle used for describing the rotation of the helix along its axis in Fig 3C is defined in[68] as the dihedral angle identified by the position of the four center of mass of the following atom groups:

Group1: residues Val8, Val9, Thr32, Phe33, Leu52, Ser53, Ile80

Group2: residues Leu87, Asp88, Ala89, and Ala90

Group3: residues Val91, Ser92, Ala93, and Tyr94

Group4: residues Asp88, Val91 and Ser92

$\Delta\delta^{15}N$ were computed for Fig. S2 and Fig. S3 with Sparta+[37] for the three possible exchange processes: $t \Leftrightarrow g-$; $g+ \Leftrightarrow g-$; and average $t,g+ \Leftrightarrow g-$. For each of the single states (t, $g+$ and $g-$) the chemical shifts have been averaged over 5000 frames extracted from the simulation.

Supplementary Material

Refer to Web version on PubMed Central for supplementary material.

Acknowledgements

We thank Dr. Lewis E. Kay at the University of Toronto for the R_1^{HzNz} pulse sequence and the NHMFL with support from NSF for NMR time. The simulations on Anton were performed as part of allocation PSCA00059 from NRBSC/PSC and supported by NIH RC2GM093307 awarded to the NRBSC. We also gratefully acknowledge support by the NRBSC/PSC staff. This work was supported by the Howard Hughes Medical Institute, the Office of Basic Energy Sciences, Catalysis Science Program, U.S. Dept. of Energy, award DE-FG02-05ER15699, and NIH (GM100966-01). We also gratefully acknowledge support by the NRBSC/PSC staff and additional computer time from XSEDE resources.

References

1. Volkman BF, Lipson D, Wemmer DE, Kern D. Two-state allosteric behavior in a single-domain signaling protein. Science. 2001; 291:2429–2433. [PubMed: 11264542]
2. Gardino AK, Villali J, Kivenson A, Lei M, Liu CF, Steindel P, Eisenmesser EZ, Labeikovsky W, Wolf-Watz M, Clarkson MW, Kern D. Transient Non-native Hydrogen Bonds Promote Activation of a Signaling Protein. Cell. 2009; 139:1109–1118. [PubMed: 20005804]
3. Keener J, Kustu S. Protein-Kinase and Phosphoprotein Phosphatase-Activities of Nitrogen Regulatory Proteins Ntrb and Ntrc of Enteric Bacteria - Roles of the Conserved Amino-Terminal Domain of Ntrc. Proceedings of the National Academy of Sciences of the United States of America. 1988; 85:4976–4980. [PubMed: 2839825]
4. De Carlo S, Chen BY, Hoover TR, Kondrashkina E, Nogales E, Nixon BT. The structural basis for regulated assembly and function of the transcriptional activator NtrC. Genes & Development. 2006; 20:1485–1495. [PubMed: 16751184]
5. Weiss DS, Batut J, Klose KE, Keener J, Kustu S. The Phosphorylated Form of the Enhancer-Binding Protein Ntrc Has an Atpase Activity That Is Essential for Activation of Transcription. Cell. 1991; 67:155–167. [PubMed: 1833069]
6. Su W, Porter S, Kustu S, Echols H. DNA-Looping and Enhancer Activity - Association between DNA-Bound Ntrc Activator and Rna-Polymerase at the Bacterial Glna Promoter. Proceedings of the

National Academy of Sciences of the United States of America. 1990; 87:5504–5508. [PubMed: 2164685]

7. Kern D, Zuiderweg ERP. The role of dynamics in allosteric regulation. Current Opinion in Structural Biology. 2003; 13:748–757. [PubMed: 14675554]
8. Cho HS, Lee SY, Yan DL, Pan XY, Parkinson JS, Kustu S, Wemmer DE, Pelton JG. NMR structure of activated CheY. Journal of Molecular Biology. 2000; 297:543–551. [PubMed: 10731410]
9. Volz K. Structural Conservation in the Chey Superfamily. Biochemistry. 1993; 32:11741–11753. [PubMed: 8218244]
10. Volz K, Matsumura P. Crystal-Structure of Escherichia-Coli Chey Refined at 1.7-a Resolution. Journal of Biological Chemistry. 1991; 266:15511–15519. [PubMed: 1869568]
11. Simonovic M, Volz K. A distinct meta-active conformation in the 1.1-angstrom resolution structure of wild-type apoCheY. Journal of Biological Chemistry. 2001; 276:28637–28640. [PubMed: 11410584]
12. Zhu XY, Rebello J, Matsumura P, Volz K. Crystal structures of CheY mutants Y106W and T871/Y106W - CheY activation correlates with movement of residue 106. Journal of Biological Chemistry. 1997; 272:5000–5006. [PubMed: 9030562]
13. Dyer CM, Dahlquist FW. Switched or not?: the structure of unphosphorylated CheY bound to the N terminus of FliM. Journal of Bacteriology. 2006; 188:7354–7363. [PubMed: 17050923]
14. Stock AM, Guhaniyogi J. A new perspective on response regulator activation. Journal of Bacteriology. 2006; 188:7328–7330. [PubMed: 17050920]
15. Birck C, Mourey L, Gouet P, Fabry B, Schumacher J, Rousseau P, Kahn D, Samama JP. Conformational changes induced by phosphorylation of the FixJ receiver domain. Structure with Folding & Design. 1999; 7:1505–1515. [PubMed: 10647181]
16. Zhao XD, Copeland DM, Soares AS, West AH. Crystal structure of a complex between the phosphorelay protein YPD1 and the response regulator domain of SLN1 bound to a phosphoryl analog. Journal of Molecular Biology. 2008; 375:1141–1151. [PubMed: 18076904]
17. Ahn DR, Song H, Kim J, Lee S, Park S. The crystal structure of an activated Thermotoga maritima CheY with N-terminal region of FliM. International Journal of Biological Macromolecules. 2013; 54:76–83. [PubMed: 23237794]
18. Park AK, Moon JH, Lee KS, Chi YM. Crystal structure of receiver domain of putative NarL family response regulator spr1814 from Streptococcus pneumoniae in the absence and presence of the phosphoryl analog beryllofluoride. Biochemical and Biophysical Research Communications. 2012; 421:403–407. [PubMed: 22521891]
19. Hastings CA, Lee SY, Cho HS, Yan DL, Kustu S, Wemmer DE. High-resolution solution structure of the beryllofluoride-activated NtrC receiver domain. Biochemistry. 2003; 42:9081–9090. [PubMed: 12885241]
20. Knaggs MH, Salsbury FR, Edgell MH, Fetrow JS. Insights into correlated motions and long-range interactions in CheY derived from molecular dynamics simulations. Biophysical Journal. 2007; 92:2062–2079. [PubMed: 17172298]
21. Roche P, Mouawad L, Perahia D, Samama JP, Kahn D. Molecular dynamics of the FixJ receiver domain: movement of the β4-α4 loop correlates with the in and out flip of Phe101. Protein Science. 2002; 11:2622–2630. [PubMed: 12381845]
22. Itoh K, Sasai M. Statistical mechanics of protein allostery: Roles of backbone and side-chain structural fluctuations. Journal of Chemical Physics. 2011; 134
23. Liu MS, Todd BD, Yao SG, Feng ZP, Norton RS, Sadus RJ. Coarse-grained dynamics of the receiver domain of NtrC: Fluctuations, correlations and implications for allosteric cooperativity. Proteins-Structure Function and Bioinformatics. 2008; 73:218–227.
24. Pandini A, Fornili A, Fraternali F, Kleinjung J. Detection of allosteric signal transmission by information-theoretic analysis of protein dynamics. Faseb Journal. 2012; 26:868–881. [PubMed: 22071506]
25. Formaneck MS, Ma L, Cui Q. Reconciling the “old” and “new” views of protein allostery: A molecular simulation study of chemotaxis Y protein (CheY). Proteins-Structure Function and Bioinformatics. 2006; 63:846–867.

26. Ma L, Cui Q. Activation mechanism of a signaling protein at atomic resolution from advanced computations. Journal of the American Chemical Society. 2007; 129:10261–10268. [PubMed: 17655236]
27. McDonald LR, Whitley MJ, Boyer JA, Lee AL. Colocalization of Fast and Slow Timescale Dynamics in the Allosteric Signaling Protein CheY. Journal of Molecular Biology. 2013; 425:2372–2381. [PubMed: 23648838]
28. Bourret RB. Receiver domain structure and function in response regulator proteins. Current Opinion in Microbiology. 2010; 13:142–149. [PubMed: 20211578]
29. Loria JP, Rance M, Palmer AG. A relaxation-compensated Carr-Purcell-Meiboom-Gill sequence for characterizing chemical exchange by NMR spectroscopy. Journal of the American Chemical Society. 1999; 121:2331–2332.
30. Vallurupalli P, Hansen DF, Stollar E, Meirovitch E, Kay LE. Measurement of bond vector orientations in invisible excited states of proteins. Proceedings of the National Academy of Sciences of the United States of America. 2007; 104:18473–18477. [PubMed: 18006656]
31. Gardino AK, Kern D. Functional dynamics of response regulators using NMR relaxation techniques. Methods in Enzymology. 2007; 423:149–167. [PubMed: 17609130]
32. Loria JP, Berlow RB, Watt ED. Characterization of enzyme motions by solution NMR relaxation dispersion. Accounts of Chemical Research. 2008; 41:214–221. [PubMed: 18281945]
33. Kleckner IR, Foster MP. An introduction to NMR-based approaches for measuring protein dynamics. Biochimica Et Biophysica Acta-Proteins and Proteomics. 2011; 1814:942–968.
34. Moorthy BS, Anand GS. Multistate Allostery in Response Regulators: Phosphorylation and Mutagenesis Activate RegA via Alternate Modes. Journal of Molecular Biology. 2012; 417:468–487. [PubMed: 22326871]
35. Halkides CJ, McEvoy MM, Casper E, Matsumura P, Volz K, Dahlquist FW. The 1.9 A resolution crystal structure of phosphono-CheY, an analogue of the active form of the response regulator, CheY. Biochemistry. 2000; 39:5280–6. [PubMed: 10819997]
36. Hu JS, Grzesiek S, Bax A. Two-dimensional NMR methods for determining (chi 1) angles of aromatic residues in proteins from three-bond J(C'C gamma) and J(NC gamma) couplings. Journal of the American Chemical Society. 1997; 119:1803–1804.
37. Shen Y, Bax A. SPARTA plus: a modest improvement in empirical NMR chemical shift prediction by means of an artificial neural network. Journal of Biomolecular Nmr. 2010; 48:13–22. [PubMed: 20628786]
38. Unruh JR, Liyanage MR, Johnson CK. Tyrosyl rotamer interconversion rates and the fluorescence decays of N-acetyltyrosinamide and short tyrosyl peptides. Journal of Physical Chemistry B. 2007; 111:5494–5502.
39. Wuthrich K, Wagner G. NMR investigations of dynamics of aromatic amino-acid residues in basic pancreatic trypsin inhibitor. Febs Letters. 1975; 50:265–268. [PubMed: 234403]
40. Keller RM, Wuthrich K. H-1 NMR-studies at 360MHz of aromatic amino-acid residues in ferrocytorchrome C-552 from Euglena-Gracilis. Biochimica Et Biophysica Acta. 1977; 491:416–422. [PubMed: 192308]
41. Skalicky JJ, Mills JL, Sharma S, Szyperski T. Aromatic ring-flipping in supercooled water: Implications for NMR-based structural biology of proteins. Journal of the American Chemical Society. 2001; 123:388–397. [PubMed: 11456540]
42. Kasinath V, Valentine KG, Wand AJ. A C-13 Labeling Strategy Reveals a Range of Aromatic Side Chain Motion in Calmodulin. Journal of the American Chemical Society. 2013; 135:9560–9563. [PubMed: 23767407]
43. Barakat M, Ortet P, Whitworth DE. P2CS: a database of prokaryotic two-component systems. Nucleic Acids Research. 2011; 39:D771–D776. [PubMed: 21051349]
44. Yan D, Cho HS, Hastings CA, Igo MM, Lee SY, Pelton JG, Stewart V, Wemmer DE, Kustu S. Beryllofluoride mimics phosphorylation of NtrC and other bacterial response regulators. Proc Natl Acad Sci U S A. 1999; 96:14789–94. [PubMed: 10611291]
45. Zhu XY, Amsler CD, Volz K, Matsumura P. Tyrosine 106 of CheY plays an important role in chemotaxis signal transduction in Escherichia coli. Journal of Bacteriology. 1996; 178:4208–4215. [PubMed: 8763950]

46. Dyer CM, Quillin ML, Campos A, Lu J, McEnvoy MM, Hausrath AC, Westbrook EM, Matsumura P, Matthews BW, Dahlquist FW. Structure of the constitutively active double mutant CheYD13K Y106W alone and in complex with a FliM peptide. Journal of Molecular Biology. 2004; 39:1325–35. [PubMed: 15351654]
47. Kanamaru K, Mizuno T. Signal Transduction and Osmoregulation in Escherichia-Coli - a Novel Mutant of the Positive Regulator, Ompr, That Functions in a Phosphorylation-Independent Manner. Journal of Biochemistry. 1992; 111:425–430. [PubMed: 1618729]
48. Osawa M, Takeuchi K, Ueda T, Nishida N, Shimada I. Functional dynamics of proteins revealed by solution NMR. Current Opinion in Structural Biology. 2012; 22:660–669. [PubMed: 23000032]
49. Mittermaier A, Kay LE. Review - New tools provide new insights in NMR studies of protein dynamics. Science. 2006; 312:224–228. [PubMed: 16614210]
50. Palmer AG. NMR probes of molecular dynamics: Overview and comparison with other techniques. Annual Review of Biophysics and Biomolecular Structure. 2001; 30:129–155.
51. Korzhnev DM, Neudecker P, Mittermaier A, Orekhov VY, Kay LE. Multiple-site exchange in proteins studied with a suite of six NMR relaxation dispersion experiments: An application to the folding of a Fyn SH3 domain mutant. Journal of the American Chemical Society. 2005; 127:15602–15611. [PubMed: 16262426]
52. Grey MJ, Wang CY, Palmer AG. Disulfide bond isomerization in basic pancreatic trypsin inhibitor: Multisite chemical exchange quantified by CPMG relaxation dispersion and chemical shift modeling. Journal of the American Chemical Society. 2003; 125:14324–14335. [PubMed: 14624581]
53. Fraser JS, Clarkson MW, Degnan SC, Erion R, Kern D, Alber T. Hidden alternative structures of proline isomerase essential for catalysis. Nature. 2009; 462:669–673. [PubMed: 19956261]
54. Eisenmesser EZ, Millet O, Labeikovsky W, Korzhnev DM, Wolf-Watz M, Bosco DA, Skalicky JJ, Kay LE, Kern D. Intrinsic dynamics of an enzyme underlies catalysis. Nature. 2005; 438:117–121. [PubMed: 16267559]
55. Korzhnev DM, Salvatella X, Vendruscolo M, Di Nardo AA, Davidson AR, Dobson CM, Kay LE. Low-populated folding intermediates of Fyn SH3 characterized by relaxation dispersion NMR. Nature. 2004; 430:586–590. [PubMed: 15282609]
56. Neudecker P, Zarrine-Afsar A, Davidson AR, Kay LE. Phi-Value analysis of a three-state protein folding pathway by NMR relaxation dispersion spectroscopy. Proceedings of the National Academy of Sciences of the United States of America. 2007; 104:15717–15722. [PubMed: 17898173]
57. McDonald LR, Boyer JA, Lee AL. Segmental Motions, Not a Two-State Concerted Switch, Underlie Allostery in CheY. Structure. 2012; 20:1363–1373. [PubMed: 22727815]
58. Mo G, Zhou H, Kawamura T, Dahlquist FW. Solution structure of a complex of the histidine autokinase CheA with its substrate CheY. Biochemistry. 2012; 51:3786–3798. [PubMed: 22494339]
59. McEvoy MM, Bren A, Eisenbach M, Dahlquist FW. Identification of the binding interfaces on CheY for two of its targets, the phosphatase CheZ and the flagellar switch protein fliM. J Mol Biol. 1999; 289:1423–33. [PubMed: 10373376]
60. Mulder FAA, Mittermaier A, Hon B, Dahlquist FW, Kay LE. Studying excited states of proteins by NMR spectroscopy. Nature Structural Biology. 2001; 8:932–935.
61. Palmer AG, Kroenke CD, Loria JP. Nuclear magnetic resonance methods for quantifying microsecond-to-millisecond motions in biological macromolecules. Methods in Enzymology. 2001; 339:204–238. [PubMed: 11462813]
62. Tollinger M, Skrynnikov NR, Mulder FAA, Forman-Kay JD, Kay LE. Slow dynamics in folded and unfolded states of an SH3 domain. Journal of the American Chemical Society. 2001; 123:11341–11352. [PubMed: 11707108]
63. Delaglio F, Grzesiek S, Vuister GW, Zhu G, Pfeifer J, Bax A. Nmrpipe - a Multidimensional Spectral Processing System Based on Unix Pipes. Journal of Biomolecular Nmr. 1995; 6:277–293. [PubMed: 8520220]

64. Wang CY, Rance M, Palmer AG. Mapping chemical exchange in proteins with MW > 50 kD. Journal of the American Chemical Society. 2003; 125:8968–8969. [PubMed: 15369325]

65. Farrow NA, Muhandiram R, Singer AU, Pascal SM, Kay CM, Gish G, Shoelson SE, Pawson T, Formankay JD, Kay LE. Backbone Dynamics of a Free and a Phosphopeptide-Complexed Src Homology-2 Domain Studied by N-15 Nmr Relaxation. Biochemistry. 1994; 33:5984–6003. [PubMed: 7514039]

66. Pelton JG, Kustu S, Wemmer DE. Solution structure of the DNA-binding domain of NtrC with three alanine substitutions. Journal of Molecular Biology. 1999; 292:1095–1110. [PubMed: 10512705]

67. Hess HH, Derr JE. Assay of inorganic and organic phosphorous in 0.1-5 nanomole range. Analytical Biochemistry. 1975; 63:607–613. [PubMed: 1122033]

68. Lei M, Velos J, Gardino A, Kivenson A, Karplus M, Kern D. Segmented Transition Pathway of the Signaling Protein Nitrogen Regulatory Protein C. Journal of Molecular Biology. 2009; 392:823–836. [PubMed: 19576227]

69. MacKerell AD, Bashford D, Bellott M, Dunbrack RL, Evanseck JD, Field MJ, Fischer S, Gao J, Guo H, Ha S, Joseph-McCarthy D, Kuchnir L, Kuczera K, Lau FTK, Mattos C, Michnick S, Ngo T, Nguyen DT, Prodhom B, Reiher WE, Roux B, Schlenkrich M, Smith JC, Stote R, Straub J, Watanabe M, Wiorkiewicz-Kuczera J, Yin D, Karplus M. All-atom empirical potential for molecular modeling and dynamics studies of proteins. Journal of Physical Chemistry B. 1998; 102:3586–3616.

70. MacKerell AD, Banavali N, Foloppe N. Development and current status of the CHARMM force field for nucleic acids. Biopolymers. 2001; 56:257–265. [PubMed: 11754339]

71. Humphrey W, Dalke A, Schulten K. VMD: Visual molecular dynamics. Journal of Molecular Graphics & Modelling. 1996; 14:33–38.

72. Phillips JC, Braun R, Wang W, Gumbart J, Tajkhorshid E, Villa E, Chipot C, Skeel RD, Kale L, Schulten K. Scalable molecular dynamics with NAMD. Journal of Computational Chemistry. 2005; 26:1781–1802. [PubMed: 16222654]

73. Brünger, AT. X-PLOR, Version 3.1: a system for X-ray crystallography and NMR. Yale University Press; New Haven: 1992.

74. Feller SE, Zhang YH, Pastor RW, Brooks BR. Contant-pressure molecular-dynamics simulation - the langevin piston method. Journal of Chemical Physics. 1995; 103:4613–4621.

75. Martyna GJ, Tobias DJ, Klein ML. Contant-pressure molecular-dynamics algorithms. Journal of Chemical Physics. 1994; 101:4177–4189.

76. Shaw DE, Deneroff MM, Dror RO, Kuskin JS, Larson RH, Salmon JK, Young C, Batson B, Bowers KJ, Chao JC, Eastwood MP, Gagliardo J, Grossman JP, Ho CR, Ierardi DJ, Kolossvary I, Klepeis JL, Layman T, Mcleavey C, Moraes MA, Mueller R, Priest EC, Shan YB, Spengler J, Theobald M, Towles B, Wang SC. Anton, a special-purpose machine for molecular dynamics simulation. Communications of the Acm. 2008; 51:91–97.

77. Shaw, DE.; Dror, RO.; Salmon, JK.; Grossman, JP.; Mackenzie, KM.; Bank, JA.; Young, C.; Deneroff, MM.; Batson, B.; Bowers, KJ.; Chow, E.; Eastwood, MP.; Ierardi, DJ.; Klepeis, JL.; Kuskin, JS.; Larson, RH.; Lindorff-Larsen, K.; Maragakis, P.; Moraes, MA.; Piana, S.; Shan, Y.; Towles, B. Proceedings of the Conference on High Performance Computing Networking, Storage and Analysis. ACM; Portland, Oregon: 2009. Millisecond-scale molecular dynamics simulations on Anton; p. 1-11.

78. Teilum K, Brath U, Lundström P, Akke M. Biosynthetic 13C Labeling of Aromatic Side Chains in Proteins for NMR Relaxation Measurements. Journal of the American Chemical Society. 2006; 128:2506–2507. [PubMed: 16492013]

79. Brath U, Akke M, Yang D, Kay LE, Mulder FAA. Functional dynamics of human FKBP12 revealed by methyl 13C rotating frame relaxation dispersion NMR spectroscopy. Journal of the American Chemical Society. 2006; 128:5718–5727. [PubMed: 16637639]

80. Edgar RC. MUSCLE: multiple sequence alignment with high accuracy and high throughput. Nucleic acids research. 2004; 32:1792–1797. [PubMed: 15034147]

Highlights

- NMR dynamics show a second process that is faster then the activation transition
- This process is related to χ_1 rotamer exchange of Y101
- MD simulations show that Y101 motion is uncorrelated with the activation transition
- Experimental data against the dominant 'Y-T coupling' mechanism of activation in NtrC

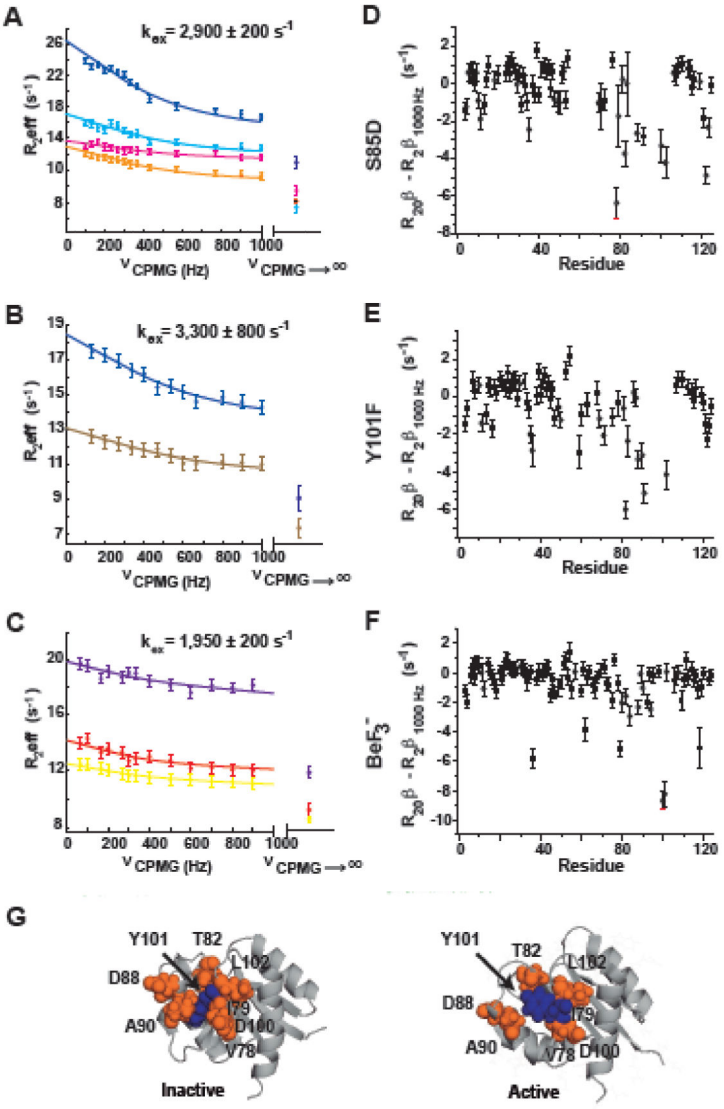

Figure 1. Y101 dynamics is kinetically independent from the inactive to active transition

(**A**-**C**) ^{15}N-CPMG relaxation dispersion profiles and $R_{20}\beta$ values for residues undergoing exchange between the inactive and active states (k_{ex}) are compared to the true exchange-free transverse relaxation rates determined independently ($R_{20}\beta$)[31] for **A**) S85D, **B**) Y101F, and **C**) BeF_3^- -activated NtrC^R. The CPMG curves refer to residues 78 (cyan), 79 (yellow), 82 (magenta), 88 (orange), 90 (light brown), 100 (purple), 101 (red), 102 (blue), and the independently determined ($R_{20}\beta$) are shown as R_2^{eff} at $\nu_{CPMG\rightarrow\infty}$. The difference between $R_{20}\beta$ and $R_2\beta_{1000Hz}$ is plotted for all amides in panels (**D**-**F**), showing that many residues sense a second fast exchange process that cannot be suppressed by the applied CPMG field strength. **G**) The residues with exchange from both processes, the inactive/active interconversion and this second faster process (orange) are clustered around Y101 (blue) in both the inactive (pdbID 1DC7) and active (pdbID 1DC8) state structures.

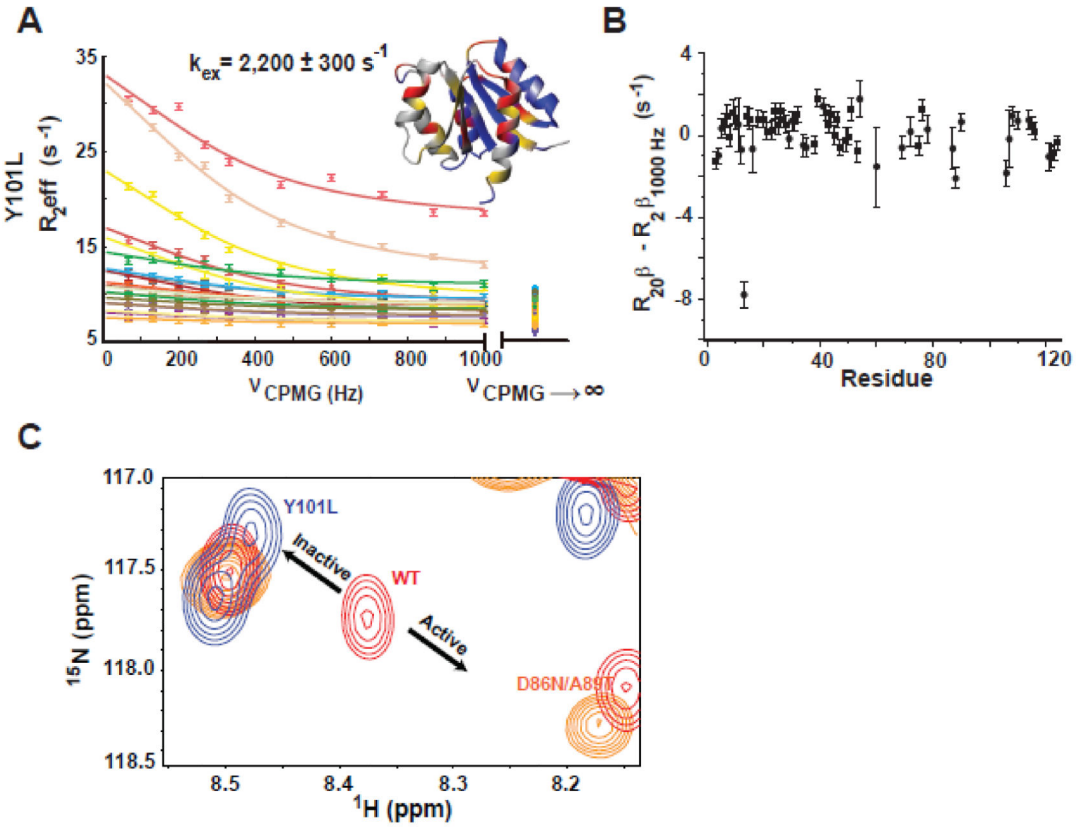

Figure 2. Y101L mutant corroborates that the faster dynamic process is due to rotamer exchange

A) ^{15}N-CPMG relaxation dispersion profiles for the Y101L NtrC^{R} mutant. Residues whose dispersion was fit globally to the fast form of the Carver-Richards equation in order to determine the rate of exchange (k_{ex}) between the inactive and active forms of the protein are shown on the structure (1DC7) in red. Yellow denotes residues whose peaks are severely exchanged broadened, residues that are flat/non-exchanging are colored in blue, and unassigned/proline/overlapped residues are in gray. Dispersion data is color coded as follows: 12 (slate), 13 (pink), 16 (rose), 30 (purple), 40 (dark grey), 41 (light orange), 54 (maroon), 60 (yellow), 68 (light pink), 78 (cyan), 87 (yellow), 88 (orange), 106 (green), 107 (dark green), 108 (olive), 110 (light yellow), 114 (tan), 115 (light green). Importantly, exchange contributions to R_2^{eff} are mostly suppressed by the applied CPMG field strength, illustrated by the difference between the exchange free transverse relaxation rates determined independently ($R_{20}\beta$ at $\nu_{CPMG\rightarrow\infty}$) and from ^{15}N-CPMG dispersion experiments ($R_2\beta_{1000Hz}$) (**B**). **C**) The Y101L mutation (blue) shifts the inactive/active state equilibrium toward the inactive state compared to WT (red) as highlighted in the ^{15}N-HSQC overlay for residue 88. The 50% active D86N/A89T mutation is shown in orange for comparison.

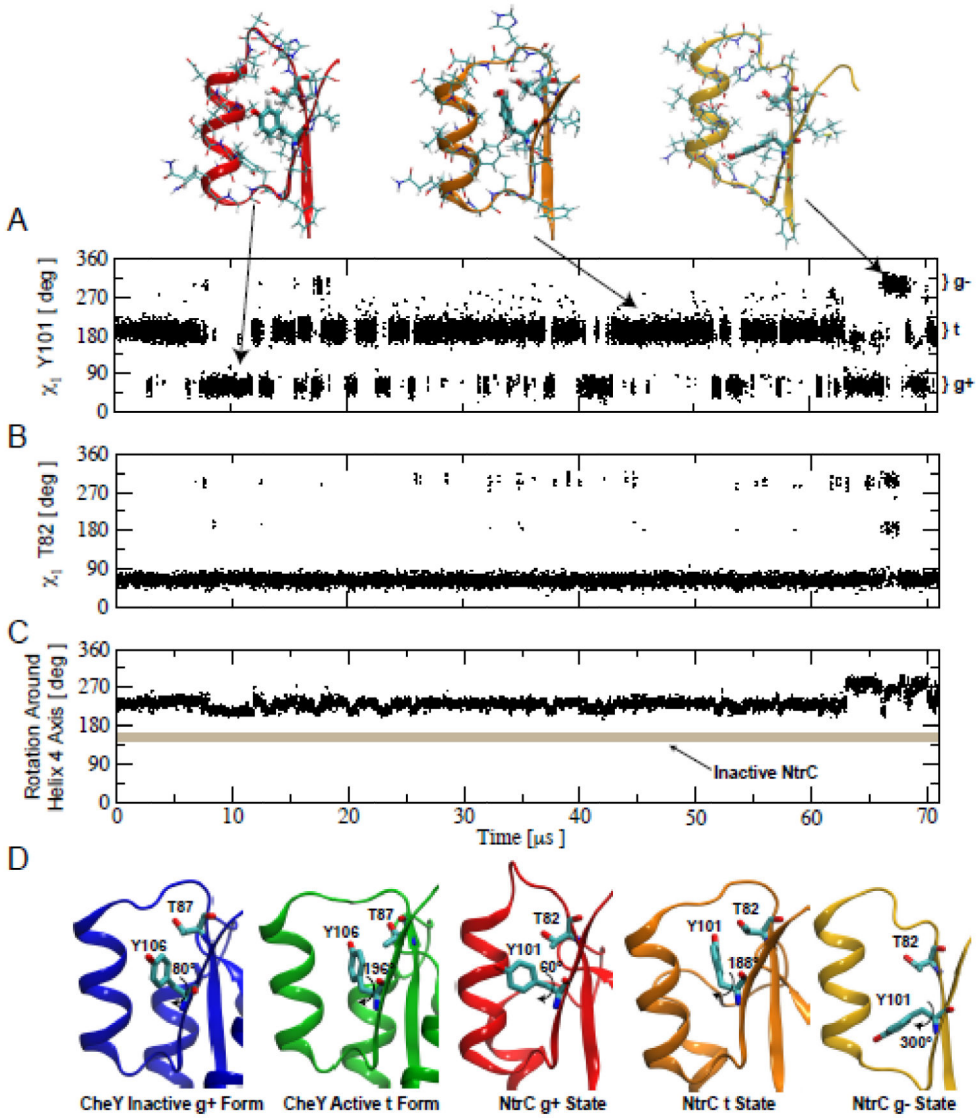

Figure 3. Within the active state several rotameric states are accessible to Y101

A) Time series of the χ_1 angle of Y101 measured along a 71 μs long molecular dynamics simulation of the nonphosphorylated receiver domain of $NtrC^R$ in the active conformation. The region of helix α4–strand β4 is shown above for representative structures of the three Y101 rotameric regions sampled. **B)** Time series of the χ_1 angle of T82 measured along the same MD simulation. **C)** Time series of a pseudo dihedral angle reporting on the rotation of the α4–strand β4 around its axis. As a reference, the value of the same order parameter for the inactive conformation of $NtrC^R$ is shown as a thick grey line demonstrating that $NtrC^R$ does not visit the inactive conformation during the 71 μs MD simulation. **D)** Comparison between the models for the inactive and active structures of CheY with the different χ_1 angles of Y106 and the corresponding T87 orientation (pdbID 1FFG and 1FQW shown in blue and green, respectively) and the structures for the three rotameric states of Y101 with

the corresponding T87 orientations visited during the simulation of the active conformation of $NtrC^{R}$.

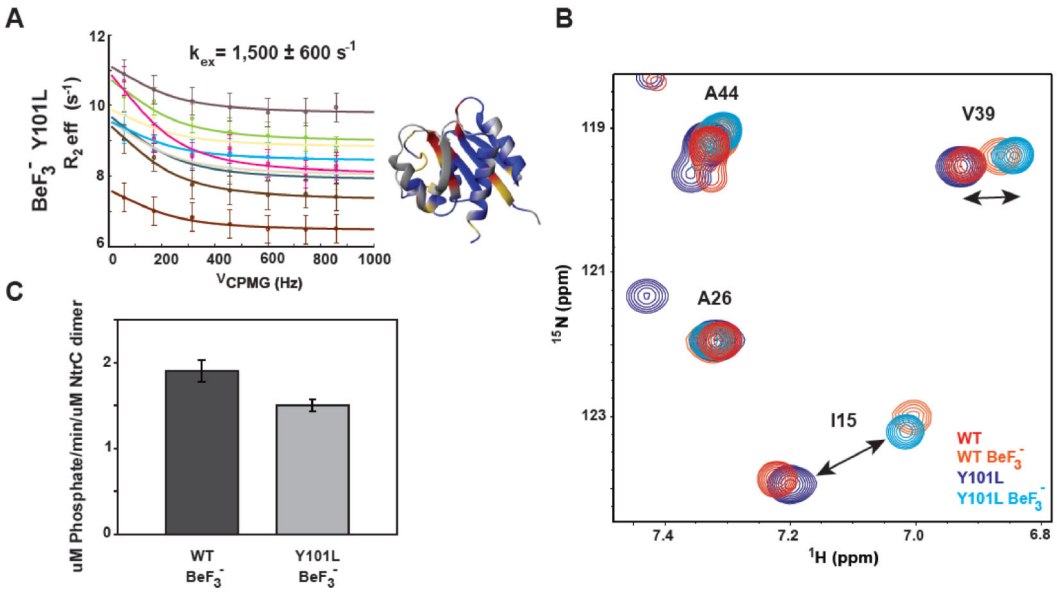

Figure 4. Mutating the conserved aromatic does not prohibit activation of the receiver domain or NtrC's downstream ATPase activity

A) ^{15}N-CPMG NMR relaxation dispersion profiles for the BeF_3^- -activated Y101L $NtrC^R$ mutant fit to a single exchange process of inactive/active interconversion. Residues whose dispersion was fit globally to determine the rate of exchange (k_{ex}) between the inactive and active forms of the protein are shown on the structure (pdbID 1DC8) in red. Yellow denotes residues whose peaks are severely exchanged broadened, residues that are flat/non-exchanging are colored in blue, and unassigned/proline/overlapped residues are in gray. Dispersion data is color coded as follows: 6 (ivory), 10 (burnt sienna), 12 (slate), 53 (tan), 64 (brown), 78 (cyan), 81 (green), 82 (magenta), 96 (purple). **B**) ^{15}N-HSQC overlay of WT, Y101L, BeF_3^- -activated WT, and BeF_3^- -activated Y101L $NtrC^R$ highlighting that the Y101L mutant has the characteristic peak shifts associated with the active state upon the addition of BeF_3^-. **C**) Full length NtrC ATPase activity assays comparing the net activity of BeF_3^- -activated WT (dark grey) and Y101L (light grey).